Cell Biol Toxicol (2025) 41:15
https://doi.org/10.1007/s10565-024-09966-2

RESEARCH

# eEF2K alleviates doxorubicin-induced cardiotoxicity by inhibiting GSK3β and improving autophagy dysfunction

**Junjie Guan · Hongwei Mo · Vicheth Virak · Runze Guo · Dongdong Que · Wenjie Yu · Xuwei Zhang · Jing Yan · Yuxi Wang · Yashu Yang · Bowen Rui · Guanlin Huang · Deshu Chen · Chongbin Zhong · Pingzhen Yang**

Received: 31 July 2024 / Accepted: 10 December 2024


**Abstract** Doxorubicin-induced cardiotoxicity (DIC) poses a threat to the health and prognosis of cancer patients. It is important to find a safe and effective method for the prevention and treatment of DIC. eEF2K, which is a highly conserved α-kinase, is thought to be a therapeutic target for several human diseases. Nonetheless, it is still uncertain if eEF2K contributes to the cardiotoxic effects caused by doxorubicin (DOX). Our research revealed that eEF2K expression decreased in the DIC. eEF2K was overexpressed through adeno-associated virus in vivo and adenovirus in vitro, which presented alleviative cardiomyocyte death and cell atrophy induced by DOX. Autophagy dysfunction is one of important mechanisms in DIC. As a result, autophagic function was evaluated using Transmission electron microscopy in vivo, as well as LysoSensor and mRFPGFP-LC3 puncta in vitro. eEF2K overexpression improves DOX-induced autophagy blockade. In addition, eEF2K knockdown aggravated autophagy blockade and cardiomyocyte injury in DIC model. eEF2K also phosphorylated and inhibited GSK3β in DIC model. AR-A014418 (ARi), known for selectively inhibiting GSK3β, countered the effects of eEF2K knockdown, which aggravated autophagy blockade in the DIC. In conclusion, this study proposes that eEF2K alleviates DIC by inhibiting GSK3β and improving autophagy dysfunction. eEF2K is a promising therapeutic target against DIC.

**Keywords** eEF2K · Doxorubicin · Cardiotoxicity · Autophagy · GSK3β

Junjie Guan, Hongwei Mo, and Vicheth Virak contributed equally to this work.

**Research highlights**
1- eEF2K is down-regulated in mouse heart and NRCMs in response to DOX.
2- eEF2K alleviates DOX-induced cardiotoxicity by alleviating autophagy impairment.
3- eEF2K phosphorylates and inhibits GSK3β, which is responsible for DOX-induced autophagy blockade.
4- eEF2K is a new therapeutic target for doxorubicin-induced cardiotoxicity.

**Supplementary Information** The online version contains supplementary material available at https://doi.org/10.1007/s10565-024-09966-2.

J. Guan · H. Mo · V. Virak · R. Guo · D. Que · W. Yu · X. Zhang · J. Yan · Y. Wang · Y. Yang · B. Rui · G. Huang · D. Chen (✉) · C. Zhong (✉) · P. Yang (✉)
Department of Cardiology, Laboratory of Heart Center, Zhujiang Hospital, Southern Medical University, No 253, Middle Gongye Avenue, 510282 Guangzhou, Guangdong, People's Republic of China
e-mail: 1834043611@qq.com

C. Zhong
e-mail: chongbinzhong@126.com

P. Yang
e-mail: y_pingzhen@126.com

Published online: 21 December 2024

## Introduction

Cardiovascular diseases and cancer are the major disease that threatens human health worldwide (Jones et al. 2012). Anti-tumor therapies, including targeted treatments and chemoradiotherapy, have significantly extended the survival of cancer patients (Yeh and Chang 2016). DOX, an anthracycline drug widely used clinically, is characterized by its cost-effectiveness and potent anti-tumor efficacy, positioning it as a cornerstone in cancer treatment regimens (Hulst et al. 2022). However, the absence of effective strategies to prevent and treat cardiotoxicity induced by DOX, limits its broader application in anti-tumor therapy (Hu et al. 2020; Singal and Iliskovic 1998).

Eukaryotic elongation factor-2 kinase (eEF2K), which is part of the α-kinase superfamily, has ancient origins that span across most eukaryotic organisms. (Piserchio et al. 2024). eEF2K is identified as a promising target for treatment across different diseases, including inflammation (Peng et al. 2023), atherosclerosis (Zhang et al. 2014), hypertension (Usui et al. 2013), pulmonary hypertension (Kameshima et al. 2015), Alzheimer's disease (Kasica et al. 2022), depression (Autry et al. 2011), and various types of cancer (Temme and Asquith 2021). eEF2K plays multiple biological functions and serves as an essential molecule in autophagy signaling transduction during cellular stress (Py et al. 2009).

Regulating autophagy, which includes the initiation, autophagosome formation, and the clearance of autophagosomes and autolysosomes, is a dynamic, complex, and multi-step process (Ikeda et al. n.d.). Emerging evidence implicates a close association between autophagy dysfunction and cardiotoxic effects of DOX (Bartlett et al. 2017). Nevertheless, DOX's influence on cardiac autophagy is determined by multiple factors, including the cardiotoxic model applied, the concentration and the duration of intervention (Bartlett et al. 2017; Dempke et al. 2023; Pan et al. 2019; Park et al. 2016; Sishi et al. 2013). In addition, the cardiomyocyte death and cell atrophy are inextricably associated with DOX-induced autophagy dysfunction (Orogo and Gustafsson 2015). Recent studies suggest that eEF2K alleviates endoplasmic reticulum stress by promoting autophagy, thereby safeguarding against myocardial cell injury induced by hypoxia (Pires Da Silva et al. 2020). These findings suggests that eEF2K represents a potential target with myocardial-protective properties. Whether eEF2K contributes to autophagy dysfunction triggered by DOX is still not clear.

This research initially focused on the biological function of eEF2K in DIC and aimed to elucidate the molecular mechanisms. Our results suggested that Glycogen Synthase Kinase 3β (GSK3β) is a downstream target of eEF2K, inactivating through phosphorylation at the Ser9 site. Our research clarified that eEF2K alleviated DIC by inhibiting GSK3β and ameliorating autophagy dysfunction, and provided a novel therapeutic target against DIC.

## Materials and methods

### Mouse adeno-associated virus infection and DIC establishment

Male C57BL/6 mice, within the age range of 6 to 8 weeks, were randomly distributed into various groups and maintained in SPF conditions, with unrestricted access to food and water, adhering to a uniform 12-h light/dark rhythm. The mice received an injection of adeno-associated virus with overexpressed eEF2K (AAV-eEF2K) through the tail vein, and the control group received an equivalent dose of empty virus (NC). After 14 days of feeding in standard animal rooms, we created an acute DIC by administering a single dose of DOX via intraperitoneal injection (MCE, HY-P2106A, 15 mg/kg), while the same volume of saline was injected into the control group. After 5 days of intervention, mice were subjected to cardiac ultrasound examination. Subsequently, we euthanized mice and collected the

J. Guan · H. Mo · V. Virak · R. Guo · D. Que · W. Yu · X. Zhang · J. Yan · Y. Wang · Y. Yang · B. Rui · G. Huang · D. Chen · C. Zhong · P. Yang
Heart Center of Zhujiang Hospital, Guangdong Provincial Biomedical Engineering Technology Research Center for Cardiovascular Disease, Guangzhou, Guangdong, People's Republic of China

J. Guan · H. Mo · V. Virak · R. Guo · D. Que · W. Yu · X. Zhang · J. Yan · Y. Wang · Y. Yang · B. Rui · G. Huang · D. Chen · C. Zhong · P. Yang
Heart Center of Zhujiang Hospital, Sino-Japanese Cooperation Platform for Translational Research in Heart Failure, Guangzhou, Guangdong, People's Republic of China

relevant samples. The Ethics Committee of Southern Medical University provided the authorization for this research (approval number: LAEC-2023–165).

### Isolation and cultivation of neonatal rat cardiomyocytes and establishment of DIC

According to earlier publications, neonatal rat cardiomyocytes (NRCMs) were isolated (Yang et al. 2023). Take the hearts from 1–2-day old Sprague–Dawley rat pups and carefully mince them. The cells were cultured in high glucose DMEM (Gibco) supplemented with 10% FBS (Procell), 100 μg/mL streptomycin (Gibco), 100 units/mL penicillin (Gibco), and 100 μmol/L BrdU (Sigma, B5002-1 g) at 37 °C in a 5% CO2 atmosphere. The cell model was established by 1 μM DOX intervened for 24 h.

### Bioinformatics analysis

We retrieved datasets (GSE206803, GSE59905 and GSE40289) from NCBI Gene Expression Omnibus. The intersection is used to identify common genes and perform heatmap analysis. Detailed information was provided in supplementary material Table S5-6.

### siRNA transfection

RIBOBIO was responsible for synthesizing the sequences of eEF2K siRNA (si-eEF2K) and negative control siRNA (NC). In Opti-MEM (Gibco) medium, 50 nM si-eEF2K or NC was blended with Lipofectamine 3000 (ThermoFisher Scientific) for 15 min. Then, according to the protocol of the reagent supplier, the specified mixture was used to transfect NRCMs. Following 6 h of co-culture, the medium was replaced and incubated for an additional 24 h for further steps. Refer to Supplementary Materials Table S3 for specific sequences.

### Overexpression adenovirus transfection

The adenovirus Ad-eEF2K was customized by GenePharma (Shanghai, China), Adenovirus containing non-specific sequences (Ad-NC) was used as a negative control. NRCMs was incubated with adenovirus (MOI = 50) for 8 h in cell culture medium containing 2% FBS in vitro. After replacing the cell culture medium, it was incubated for 48 h for the next steps.

### Immunofluorescence

The samples underwent staining with primary antibodies, combined by Alexa Fluor 488, Alexa Fluor 555 or Alexa Fluor 647-conjugated secondary antibodies. The cell nucleus is stained with Hoechst 33,342 (Beyotime, C1022). Images were taken using a Leica SP8 laser scanning confocal microscope. Furthermore, isotype control staining was performed on the heart to remove non-specific interference (Supplementary Fig. S1). The details of the antibodies could be found in Supplementary Material Table S2.

### Western blot

After extracting, protein sample was separated by SDS-PAGE, and transferred onto PVDF membranes. Then, blocking the membranes with 5% skim milk. Following the application of primary and secondary antibodies, protein bands were visualized with EnlightTM reagent.

### Reverse transcription quantitative PCR (RT-qPCR)

RT-qPCR was done following protocols that have been described earlier (Zhong et al. 2023). We Quantified the mRNA levels for target genes by the 2-ΔΔCt method, with β-actin as a normalized reference transcript. The detail of primer sequences was shown in the Supplementary Materials Table S3.

### LDH test and PI/Hoechst 33342 staining

Cardiomyocyte damage was assessed using an LDH assay and PI/Hoechst 33,342 staining. After preparing the working solution, follow the manufacturer's instructions and use the Varioskan-LUX microplate reader (Thermo) to measure the results at 490 nm. To stain the cells, NRCMs were treated with a 10 μM PI solution and a 20 μM Hoechst 33,342 solution for 15 min. The images were obtained through fluorescence microscopy and analyzed with the help of ImageJ.

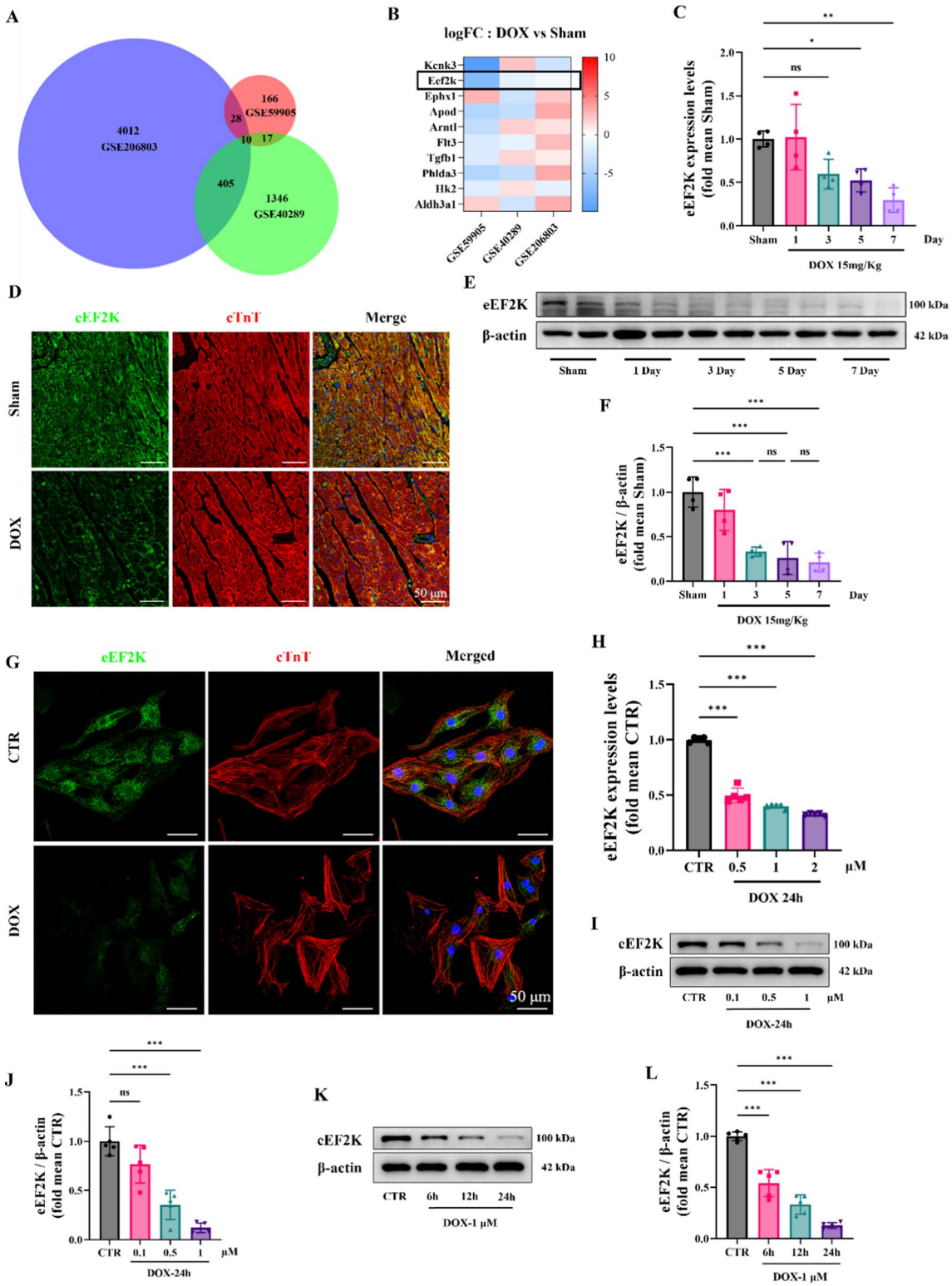
A
4012
GSE206803
166
GSE59905
28
10
17
405
1346
GSE40289
B
logFC : DOX vs Sham
Kcnk3
Eef2k
Ephx1
Apod
Arntl
Flt3
Tgfb1
Phlda3
Hk2
Aldh3a1
10
5
0
-5
GSE59905
GSE40289
GSE206803
C
eEF2K expression levels (fold mean Sham)
Sham
1
3
5
7
Day
DOX 15mg/Kg
D
cEF2K
cTnT
Merge
Sham
DOX
50 μm
E
eEF2K
β-actin
100 kDa
42 kDa
Sham
1 Day
3 Day
5 Day
7 Day
F
eEF2K / β-actin (fold mean Sham)
Sham
1
3
5
7
Day
DOX 15mg/Kg
G
cEF2K
cTnT
Merged
CTR
DOX
50 μm
H
eEF2K expression levels (fold mean CTR)
CTR
0.5
1
2
μM
DOX 24h
I
eEF2K
β-actin
100 kDa
42 kDa
CTR
0.1
0.5
1
μM
DOX-24h
J
eEF2K / β-actin (fold mean CTR)
CTR
0.1
0.5
1
μM
DOX-24h
K
eEF2K
β-actin
100 kDa
42 kDa
CTR
6h
12h
24h
DOX-1 μM
L
eEF2K / β-actin (fold mean CTR)
CTR
6h
12h
24h
DOX-1 μM

◂**Fig. 1** eEF2K was decreased in DIC. **A** The intersection of three datasets was shown by the Venn diagram. Data details could be found in Supplementary Material Table S5-S6. **B** The heatmap of the expression changes of 10 genes in three datasets was displayed. **C** The mRNA level of eEF2K in animal models was detected through RT-qPCR analysis on the 3rd, 5th, and 7th days after DOX intervention ($n=4$). **D** The expression of eEF2K in mouse heart tissue was shown by immunofluorescence staining. Green signal was used to represent eEF2K, red signal represented cTnT-labeled cardiomyocytes, and blue signal represented Hoechst 33,342-labeled nuclei. Scale bar: 50 μm. **E–F** The protein level of eEF2K in mouse heart was detected through western blot analysis, with DOX intervention as before ($n=4$). **G** The expression and distribution of eEF2K in cell DIC models were shown by immunofluorescence. Green signal was used to represent eEF2K, cTnT specifically labeled cardiomyocytes, and blue signal represented Hoechst 33,342-labeled nuclei. Scale bar: 50 μm. **H** The mRNA level of eEF2K in NRCMs was detected through a RT-qPCR analysis ($n=5$). **I-L** The protein level of eEF2K in different concentration–time gradients was detected through western blot analysis in NRCMs ($n=5$). All data are presented as mean ± standard deviation. $^{*}p<0.05$, $^{**}p<0.01$, $^{***}p<0.001$ indicate statistical differences between groups

### Phalloidin staining

As per the manufacturer's guidelines, NRCMs underwent fixation, permeabilization, and staining with phalloidin (US EVERBRIGHT, YP0063) and Hoechst 33,342, with imaging carried out by the Leica SP8 laser scanning confocal microscope. Image J was used to analyze the cell size.

### mRFP-GFP-LC3 puncta

NRCMs in a confocal dish underwent transfection with tandem fluorescent mRFP-GFP-LC3 (MOI = 15) for 8 h. Post-intervention, NRCMs were fixed with 4% paraformaldehyde and stained with Hoechst 33,342. The images were captured and documented with a Leica SP8 laser scanning confocal microscope. Ultimately, we counted the number of autophagosomes (yellow dots) and autophagosomes (red dots) in each cell.

### Fluorescent dye LysoSensor™

We used probe LysoSensor™ Yellow/Blue DND-160 (ThermoFisher, L7545) to measure lysosome levels and functionality in living cells. We stained the NRCMs with 5 μM LysoSensor™ Yellow/Blue DND-160 for 5 min after the appropriate intervention. After washing to eliminate surplus dye, the cells were immersed in PBS and promptly moved to a Leica SP8 confocal laser scanning microscope. Yellow fluorescence is emitted by LysoSensor™ Yellow/Blue DND-160 in acidic lysosomes, while blue fluorescence is emitted in neutral lysosomes. The samples were measured at 440 nm for blue and 540 nm for yellow ($I_{440}/I_{540}$).

### Echocardiography

Anesthesia was administered to the mice using 2% Pentobarbital, followed by M-mode echocardiography using the Vevo 2100 system from VisualSonics to evaluate the LVFS and LVEF.

### ELISA assay

To assess myocardial injury, serum levels of cTnT and CK-MB isoenzyme were measured. Blood samples were taken from the retroorbital venous plexus and analyzed following the manufacturer's instructions.

### Heart weight (HW) and tibia length (TL)

The degree of heart atrophy was evaluated by calculating the ratio of heart weight to tibial length (HW/TL).

### Hematoxylin and eosin (HE) staining

The heart specimens were first conserved using 4% paraformaldehyde, then subjected to an ethanol dehydration process. Following this, the ethanol was eliminated using xylene, and the samples were subsequently encapsulated in paraffin. Heart tissue embedded in paraffin was then cut into sections of 4 μm thickness. Post wax removal, the tissue sections were treated with hematoxylin and eosin for staining. Upon visualization and image capture of the heart sections with an optical microscope, the cross-sectional area of the heart was quantified utilizing Image J software.

### Wheat germ agglutinin (WGA) staining

The slices from the heart tissue were subjected to a dewaxing process, followed by staining with Wheat

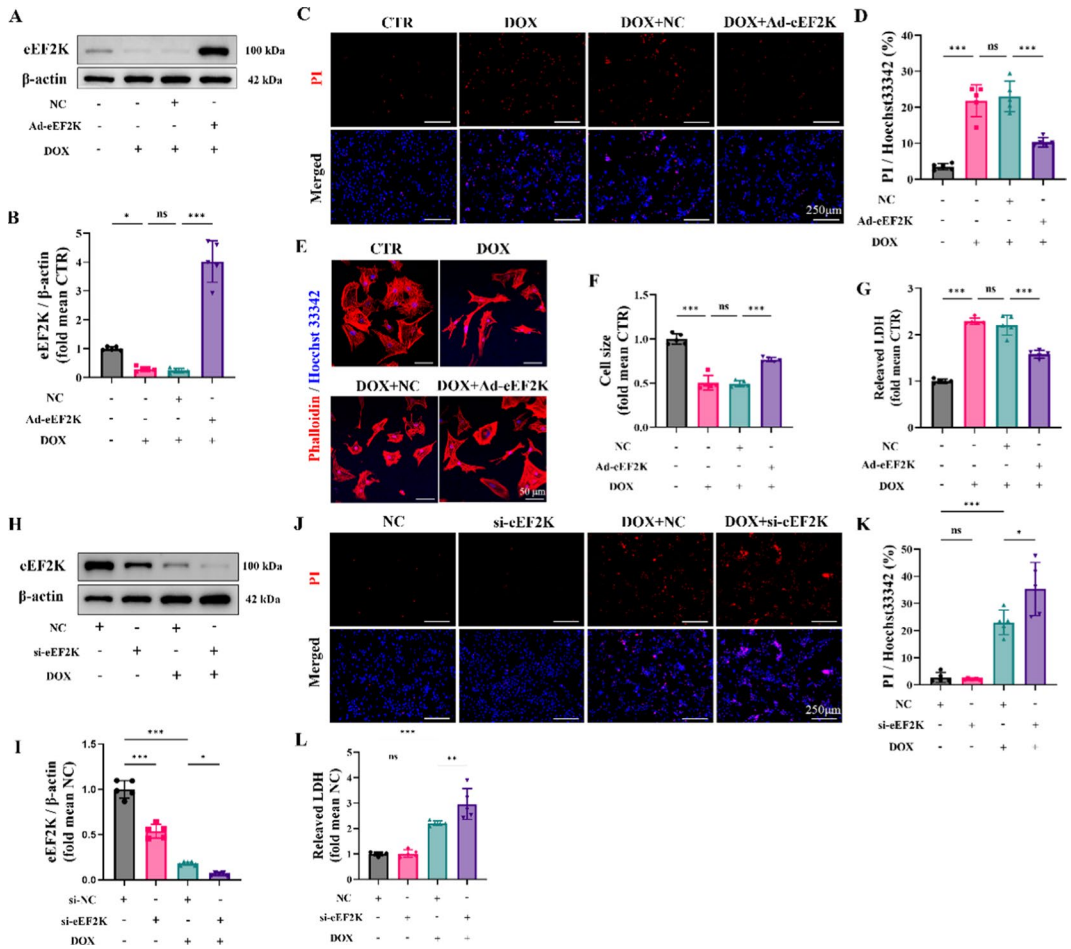


**Fig. 2** eEF2K attenuated doxorubicin-induced cardiotoxicity in NRCMs. **A-B** The levels of eEF2K protein in NRCMs by western blot analysis ($n=5$). **C-D** PI/Hoechst 33,342 staining indicated the cellular injury ($n=5$). The ratio of PI-positive cells to Hoechst 33,342-positive cells was calculated by ImageJ software to indicate the cellular injury. The scale bar represents 250 μm. **E–F** The cardiomyocyte outline was determined by phalloidin staining. Cardiomyocyte size was quantified by ImageJ software. Hoechst 33,342 staining marks the nuclei, scale bar: 50 μm. **G** Myocardial cell injury was assessed by LDH detection ($n=5$). **H-I** The levels of eEF2K protein in NRCMs by western blot analysis ($n=5$). **J-K** PI/Hoechst 33,342 staining indicated the cellular injury after eEF2K knockdown ($n=5$), scale bar: 250 μm. **L** Myocardial cell injury was assessed by LDH detection ($n=5$). All data are presented as mean ± standard deviation. $*p<0.05$, $**p<0.01$, $***p<0.001$ indicate statistical differences between groups

Germ Agglutinin (WGA, ThermoFisher, W11261) and Hoechst 33,342. Subsequent imaging was performed using a Leica SP8 confocal laser scanning microscope. The quantification of the images was accomplished with the assistance of Image J software.

## Transmission electron microscopy (TEM)

Heart tissue was swiftly harvested and cut into fragments of $1mm^3$. Following the steps of fixation, dehydration, and staining, these samples were segmented into minute grids. They were then examined using a Philips CM 10 electron microscope operating at 80 kV. The phrase 'autophagic vacuoles' is inclusive of both 'autophagosomes' and 'autolysosomes'. The count of these autophagic vacuoles was recorded and a comparative analysis was carried out among all groups.

## Statistical analysis

The statistical examination of the data was performed using the GraphPad Prism 9.0 software.

The data, which were collected from at least four independent parallel experiments, were represented as mean ± SEM. For statistical assessment, a one-way ANOVA was employed, followed by Tukey's posthoc test. The significance of the data was represented as non-significant (ns), $*p < 0.05$, $**p < 0.01$, and $***p < 0.001$, and any values falling under these categories were deemed statistically significant.

## Results

### eEF2K was decreased in DIC

DIC dataset was analyzed online on the GEO database. Differential gene expression was assessed across three RNA-seq datasets, identifying 10 differentially genes (Fig. 1 A). Detailed dataset information was provided (supplementary material Table S5-6). Heatmap analysis of these 10 genes revealed a downregulation of eEF2K (Fig. 1 B). Subsequently, an animal model of acute DIC (15 mg/kg) was established. Through RT-qPCR, we confirmed that eEF2K expression was downregulated in mouse heart at the mRNA level on the 3rd, 5th, and 7th days after DOX intervention (Fig. 1 C). Continuous stimulation with dox resulted in decreased expression of eEF2K over time (Fig. 1 E, F). According to previous literature reports (Chen et al. 2022a; Yang et al. 2023), a 5-day DOX intervention protocol was selected for subsequent animal experiments. Immunofluorescence staining also revealed that eEF2K was decreased by DOX in mouse heart (Fig. 1 D). According to RT-qPCR analysis, we found that eEF2K was decreased by DOX at the mRNA level in vitro (Fig. 1 H). The different concentrations of DOX were used, which resulted in a dose-dependent reduction of eEF2K expression (Fig. 1 I, J). Given that DOX concentrations exceeding 2 μM are not clinically relevant (Li et al. 2016), a concentration of 1 μM DOX was employed. Furthermore, the different-times intervention of DOX was used, which suggested that there was a time-dependent decrease of eEF2K at the protein level (Fig. 1 K, L). Immunofluorescence of NRCMs also revealed a reduction of eEF2K induced by DOX (Fig. 1 G).

### eEF2K attenuated doxorubicin-induced cardiotoxicity in NRCMs

To study the function of eEF2K in DIC, we utilized adenovirus to artificially enhance its expression in vitro (Supplementary Fig. S2 A, B). According to western blot analysis, eEF2K levels were lowered by DOX, yet adenovirus-mediated overexpression reinstated them. (Fig. 2 A, B). PI/Hoechst 33,342 staining demonstrated that DOX induced cardiomyocyte injury and death compared to that in the CTR group, but the overexpression of eEF2K reduced cardiomyocyte damage (Fig. 2 C, D). Similarly, LDH detection also suggested that the overexpression of eEF2K reduced cardiomyocyte injury induced by DOX (Fig. 2 G). Furthermore, Phalloidin staining revealed that myocardial cell area was reduced by DOX, whereas the overexpression of eEF2K attenuated DOX-induced cardiomyocyte atrophy (Fig. 2 E, F).

Secondly, eEF2K was knocked down by siRNA in vitro (Supplementary Fig. S3 A, B), and eEF2K was further reduced by si-eEF2K in DOX-treated NRCMs (Fig. 2 H, I). Although PI/Hoechst 33,342 staining revealed that eEF2K knockdown alone did not induce NRCMs injury, eEF2K knockdown exacerbated DOX-induced cardiomyocyte injury (Fig. 2 J, K). LDH detection supported these findings, indicating a exacerbation of DIC upon eEF2K knockdown (Fig. 2 L).

### Overexpression of eEF2K attenuated doxorubicin-induced cardiotoxicity in mice

Adeno-associated virus (AAV) was introduced into mice through an injection in the tail vein, which resulted in targeted overexpression of eEF2K specifically in the cardiac tissue (Supplementary Fig. S4 A-B). An equal amount of empty vector virus was administered to the negative control (NC) group. According to immunofluorescence analysis, the DOX group showed a decrease in eEF2K fluorescence intensity, whereas AAV-eEF2K infection led to an increase. (Fig. 3 A). Western blot similarly showed that cardiac eEF2K was reduced in the DOX group, but it was elevated through AAV-mediated overexpression (Fig. 3 B-C).

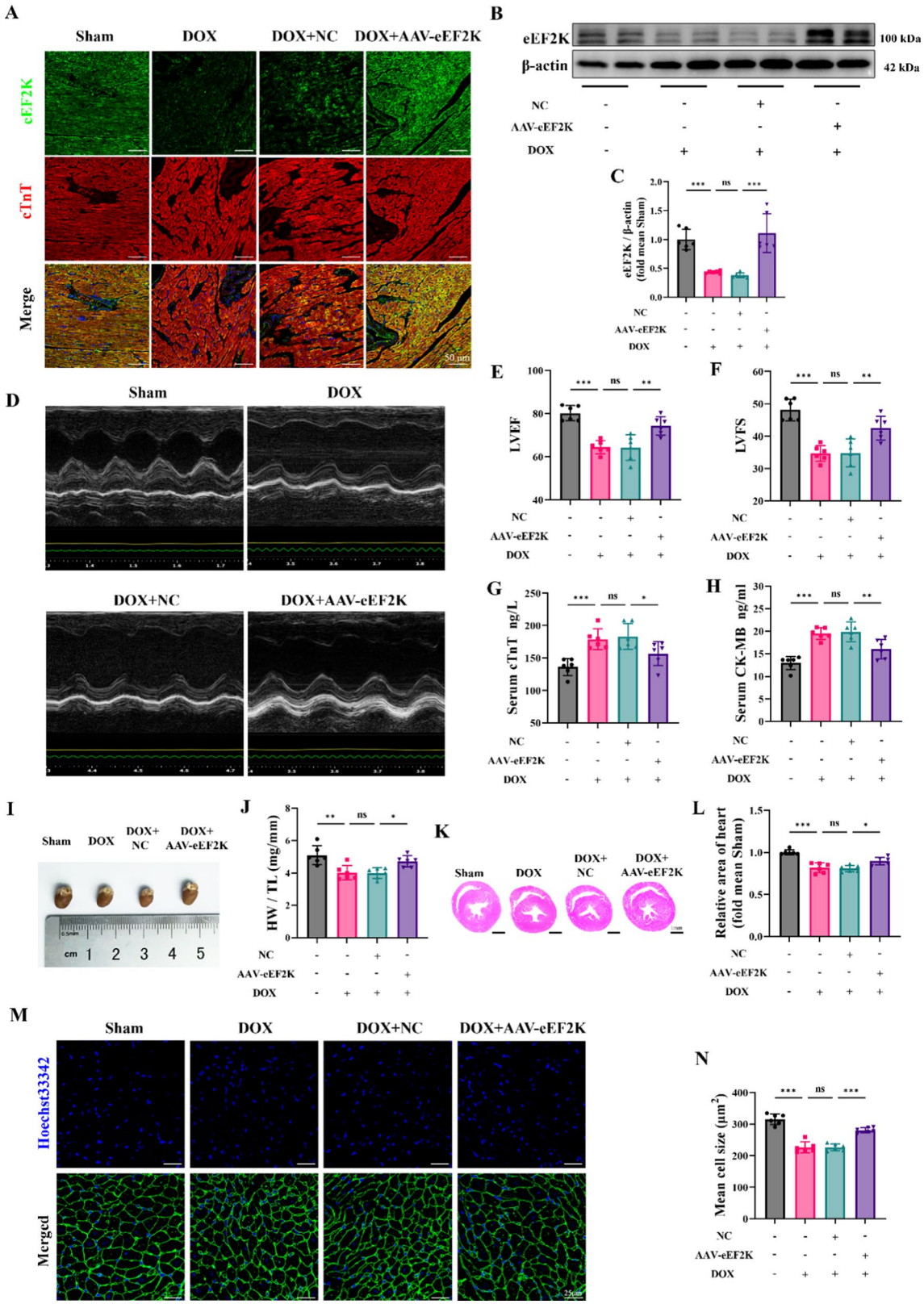
A
Sham
DOX
DOX+NC
DOX+AAV-eEF2K
eEF2K
cTnT
Merge
50 μm
B
eEF2K
β-actin
100 kDa
42 kDa
NC
AAV-eEF2K
DOX
C
eEF2K / β-actin (fold mean Sham)
D
Sham
DOX
DOX+NC
DOX+AAV-eEF2K
E
LVEF
F
LVFS
G
Serum cTnT ng/L
H
Serum CK-MB ng/ml
I
Sham
DOX
DOX+ NC
DOX+ AAV-eEF2K
cm 1 2 3 4 5
J
HW / TL (mg/mm)
K
Sham
DOX
DOX+ NC
DOX+ AAV-eEF2K
L
Relative area of heart (fold mean Sham)
M
Sham
DOX
DOX+NC
DOX+AAV-eEF2K
Hoechst33342
Merged
25μm
N
Mean cell size (μm²)

◂**Fig. 3** eEF2K attenuated doxorubicin-induced cardiotoxicity in mice. **A** Immunofluorescence analysis showed eEF2K localization in cardiac tissue. The green signal represented eEF2K, the red signal denoted cTnT-labeled cardiomyocytes, and the blue represented Hoechst 33,342-labeled nuclei. Scale bar: 50 μm. **B-C** eEF2K were detected by western blot analysis in murine cardiac tissue ($n=6$). **D-F** LVEF and LVFS were measured by short-axis M-mode echocardiography ($n=6$). **G-H** Serum cTnT and CK-MB levels were quantified by ELISA ($n=6$). **I-J** The gross heart pictures and the HW/TL ratio of mice ($n=6$). **K-L** Representative images of gross cardiac sections stained by HE stains and the cross-section area of hearts were measured ($n=6$). **M–N** Representative images stained with WGA, depicting the cross-sectional area of cardiomyocytes ($n=6$). All data are presented as mean ± standard deviation. $^{*}p<0.05$, $^{**}p<0.01$, $^{***}p<0.001$ indicate statistical differences between groups

M-mode echocardiography revealed that DOX led to a reduction in both LVEF and LVFS compared to the Sham group. In contrast, AAV-eEF2K mitigated the reduction of LVEF and LVFS caused by DOX (Fig. 3 D-F). Additionally, the DOX group had a thinner left ventricular wall, whereas wall thinning was less pronounced with DOX + AAV-eEF2K than in the DOX + NC group. (Supplementary Fig. S5 A-F). Detection of cTnT and CK-MB was used to assess myocardial injury. According to the results, DOX elevated cTnT and CK-MB levels, while AAV-eEF2K alleviated the myocardial damage induced by DOX. In the DOX + AAV-eEF2K group, cTnT and CK-MB levels were lower than those in the DOX + NC group (Fig. 3 G-H).

Because previous research has established myocardial atrophy as a principal pathological feature of DIC (Chen et al. 2022a; Ferreira de Souza et al. 2018; Lipshultz et al. 1991; Orogo and Gustafsson 2015), we evaluated the heart mass through gross cardiac specimens and the HW/TL ratio. The results suggested that both heart volume and HW/TL ratio were reduced by DOX (Fig. 3 I-J). Concurrently, we observed that there was a decline body weight following DOX intervention (Supplementary Fig. S6 A-C). However, the analysis of HW/BW ratio also indicated that AAV-eEF2K attenuated the heart mass loss induced by DOX (Supplementary Fig. S6 D). We selected heart tissue sections at the papillary muscle level for HE staining. Findings indicated a decrease in the mouse heart's cross-sectional area due to DOX, which AAV-eEF2K could help counteract (Fig. 3 K-L). Furthermore, the average cross-sectional area of cardiomyocytes was found to be smaller in the DOX group than in the Sham group, as indicated by WGA staining, and AAV-eEF2K could attenuate the cardiomyocyte atrophy induced by DOX (Fig. 3 M–N).

## eEF2K attenuated autophagy dysfunction induced by DOX

For additional confirmation, NRCMs were transfected with tandem mRFP-GFP-LC3 adenovirus to observe the number of autophagosomes and autolysosomes in vitro. Between the groups, the number of autophagosomes showed no statistical difference. Nonetheless, DOX induced a marked increase in autolysosomes compared to the CTR group. There was no statistical difference among DOX + NC group and DOX group. The overexpression of Ad-eEF2K led to a decrease in autolysosome accumulation caused by DOX (Fig. 4 A-B), which indicated that eEF2K might mitigate the DOX-induced impairment in autolysosome degradation. Western blot also suggested that eEF2K improved the DOX-induced elevation of LC3-II, thereby attenuating autophagic dysfunction (Fig. 4 C-E).

Chloroquine (CQ), a specific autophagy inhibitor, was employed to further elucidate the autophagy flux. Compared to the CTR group, the CQ group displayed a significant rise in LC3-II, suggesting the preservation of autophagy flux in normal cells. The DOX + CQ group showed a reduction in LC3-II, suggesting a reduction of autophagy flux induced by DOX compared to that in the CQ group (Supplementary Fig. S7 A-D). Additionally, LC3-II levels rose in both the Ad-eEF2K + CQ group and the Ad-eEF2K + DOX + CQ group when compared to those not treated with chloroquine, which indicated that eEF2K could restore the decrease of autophagy flux induced by DOX (Fig. 4 F-I).

Recent research has elucidated that there was an inhibition of lysosomal acidification to inhibit autophagy flux (Li et al. 2016). Therefore, we employed the LysoSensor Yellow/Blue probe to stain lysosomes. The increase of the ratio of $I_{440}/I_{540}$ suggested that DOX led to a disruption of the lysosomal acidic environment, but Ad-eEF2K decreased the ratio and restored lysosomal acidification dysfunction induced by DOX (Fig. 4 J-M).

Additionally, our findings revealed that eEF2K knockdown elevated LC3-II accumulation induced

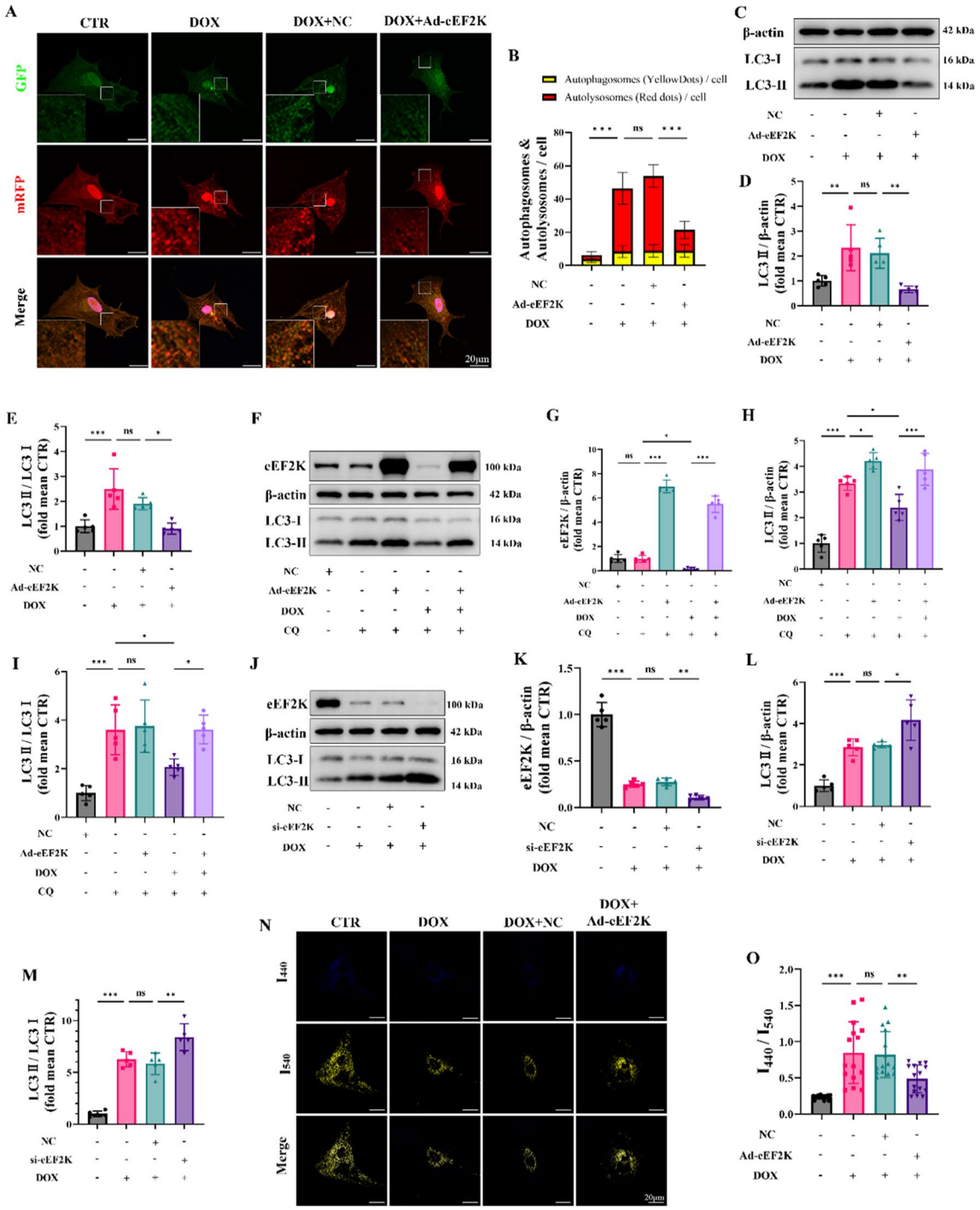


by DOX, resulting in aggravating autophagy blockade (Fig. 4 N–O). Overall, these results implicated that eEF2K restored autolysosomes accumulation and autophagy flux reduction induced by DOX, thereby attenuating DIC.

## Overexpression of eEF2K improved DOX-induced autophagy blockade in mice heart

Mice were grouped based on DOX-intervention durations, which revealed that DOX induced autophagic

◂**Fig. 4** eEF2K attenuated autophagy dysfunction in NRCMs induced by DOX. **A-B** Representative fluorescence images of NRCMs infected with mRFP-GFP-LC3 adenovirus ($n=15$). The mRFP (red) is stable in the acid organelles while the GFP (green) is not. Therefore, the green fluorescence of GFP quenched when the autophagosome fused with the lysosome to become autolysosome. The yellow dots merged by green dots and red dots represented autophagosomes and the red dots overlay no green dots indicated autolysosomes. The nuclei were stained with Hoechst 33,342 (blue). Scale bar: 20 μm. **C-E** LC3 was detected by western blot analysis in NRCMs ($n=5$). **F-I** LC3 was detected by western blot analysis following eEF2K overexpression, DOX or chloroquine intervention, reflecting the alterations of autophagy flux ($n=5$). **J-M** LC3 was detected by western blot in NRCMs ($n=5$). **N–O** Representative fluorescence images of lysosomes using LysoSensor Yellow/Blue probes ($n=15$). The blue dots with emission peak at 440 nm representing less acidic or neutral lysosomes (impaired lysosomes) as well as the yellow dots with emission peak at 540 nm indicating acid lysosomes (functional lysosomes). The ratio of $I_{440}/I_{540}$ were measured. Scale bar: 20 μm. All data are presented as mean ± standard deviation. $^{*}p<0.05$, $^{**}p<0.01$, $^{***}p<0.001$ indicate statistical differences between groups

dysfunction in mouse hearts over time, peaking at 5 days (Fig. 5 A-C). Through Western blot examination, it was found that augmenting eEF2K levels using an adenovirus led to changes in LC3-II concentrations, indicating that eEF2K could alleviate the accumulation of LC3-II instigated by DOX (Fig. 5 D-F). Furthermore, TEM was employed to evaluate the abundance of autophagic vacuoles in cardiac tissue. The results showed a low number of autophagic vacuoles in normal heart tissue, whereas DOX increased their amount. However, overexpression of eEF2K decreased the amount of autophagic vacuoles induced by DOX in cardiac tissue (Fig. 5 G-H). Collectively, these results indicate that DOX caused a blockage in cardiac autophagy, leading to the buildup of autophagic vacuoles and LC3-II, while eEF2K improved DOX-induced autophagy blockade by enhancing the degradation of autophagic vacuoles.

## eEF2K promoted GSK3β phosphorylation in DIC

Recently, eEF2K has been reported to facilitate GSK3β phosphorylation at the Ser9 site (Chen et al. 2022b). However, whether eEF2K promotes phosphorylation in DIC is still unclear.

We used western blot analysis to detect the phosphorylation level of GSK3β, revealing that DOX reduced p-GSK3β levels in vivo. However, overexpression eEF2K increased the p-GSK3β level (Fig. 6 A-C). In addition, overexpression eEF2K attenuated the reduction of p-GSK3β levels induced by DOX in vitro (Fig. 6 D-F). Similarly, eEF2K knockdown not only led to a decrease of p-GSK3β levels in normal cells, but also further decreased p-GSK3β levels in DIC (Fig. 6 G-I). These findings suggested that eEF2K promoted GSK3β phosphorylation at the Ser9 site in DIC.

## Inhibition of GSK3β reversed the effects of eEF2K knockdown on aggravating autophagy blockade in DIC

According to studies, DOX reduces the phosphorylation level at Ser9 of GSK3β, resulting in its heightened activation (Li et al. 2020; Wang et al. 2021; Zhang et al. 2020). Like previous studies, the findings indicated that the phosphorylation level of GSK3β was decreased by DOX at different concentrations intervention (Supplementary Fig. S8 D-F). The study showed that knocking down eEF2K worsens the injury to cardiomyocytes induced by DOX. Given the overactivation of GSK3β in the DIC, we used a selective GSK3β inhibitor, AR-A014418 (ARi), to investigate the therapeutic potential of inhibiting GSK3β. We found that inhibiting GSK3β could alleviate DIC (Supplementary Fig. S8 A-C). PI/Hoechst 33,342 staining showed that ARi attenuated the exacerbated cardiomyocyte injury resulting from eEF2K knockdown in DIC (Fig. 7 A-B). Similarly, LDH detection suggested that si-eEF2K notably exacerbated DIC, whereas ARi alleviated the injury (Fig. 7 C). It is worth noting that knockdown eEF2K alone did not cause damage. Furthermore, phalloidin staining demonstrated that si-eEF2K exacerbated DOX-induced cardiomyocyte atrophy, but ARi reversed the atrophic response (Fig. 7 D-E). These findings suggested that GSK3β inhibition by ARi attenuated the exacerbated cardiomyocyte injury resulting from eEF2K knockdown in DIC.

Subsequently, we investigated how ARi influences the autophagy blockade caused by DOX. The mRFP-GFP-LC3 fluorescence showed that eEF2K knockdown aggravated the accumulation of autolysosome compared to that in the DOX group, further reducing the autophagy flux. However, ARi attenuated autolysosomes accumulation and restored autophagy flux (Fig. 7 F-G). Moreover, the analysis using western

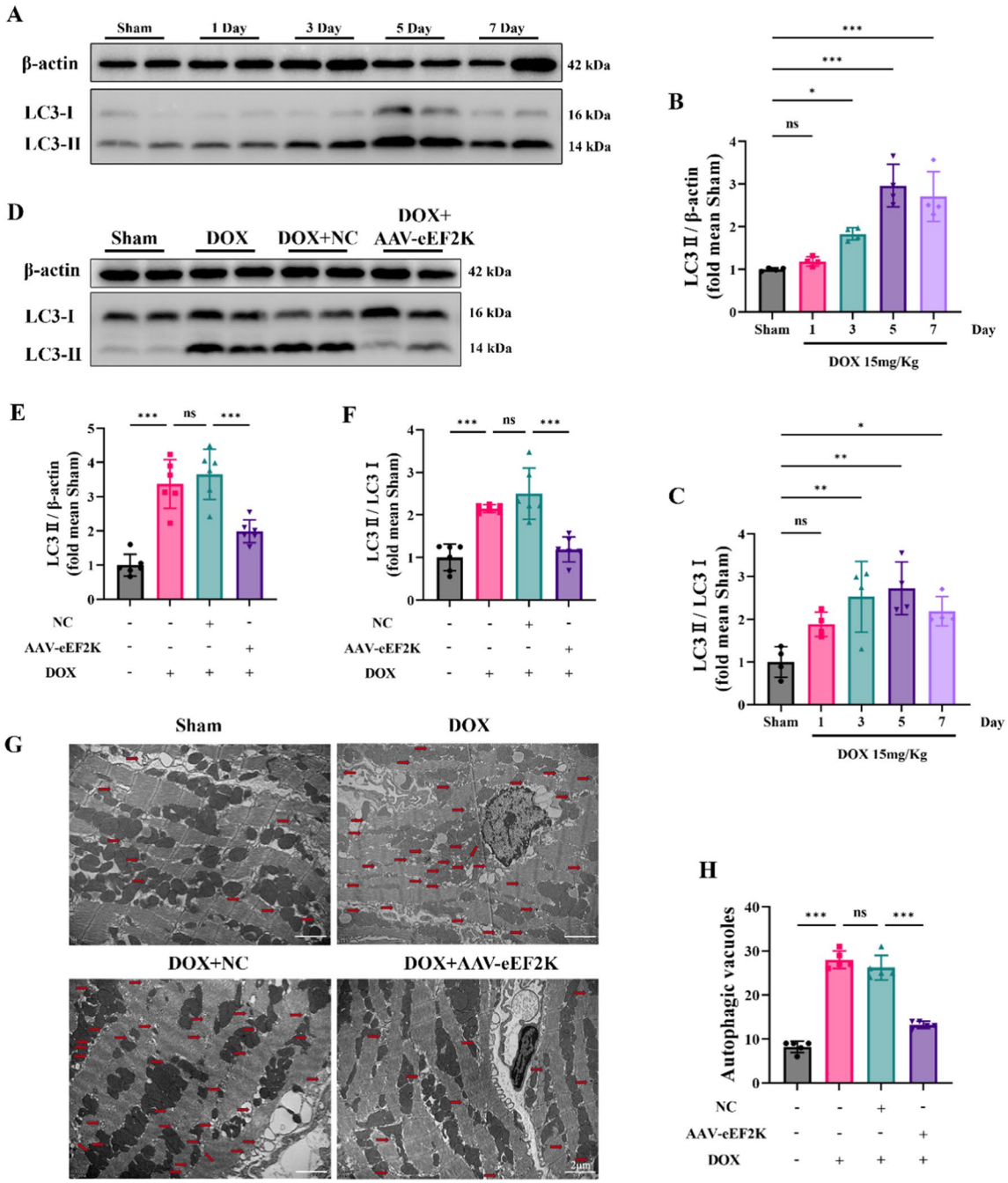


**Fig. 5** eEF2K improved DOX-induced autophagy blockade in mice heart. **A-C** LC3 was detected by western blot analysis, reflecting the impact of DOX on autophagy in mouse hearts ($n=4$). **D-F** Western blot analysis evaluated that overexpression of eEF2K attenuated the accumulation of LC3 induced by DOX ($n=6$). **G-H** Representative transmission electron microscope images of autophagic vacuoles in mouse heart ($n=5$). Autophagic vacuoles were labeled with red arrows. Scale bar: 2 μm. All data are presented as mean ± standard deviation. $^{*}p<0.05$, $^{**}p<0.01$, $^{***}p<0.001$ indicate statistical differences between groups

blot demonstrated that eEF2K knockdown resulted in elevated LC3-II levels relative to the DOX group, but LC3-II accumulation was reduced after ARi intervention (Fig. 7 H-J). These results suggested that GSK3β inhibition could attenuate the autophagy blockade induced by eEF2K knockdown in DIC.

Autophagy flux was further detected by chloroquine intervention. Our findings suggested that DOX decreased cardiomyocyte autophagy flux, and eEF2K knockdown further exacerbated this reduction. Nevertheless, the inhibition of GSK3β by ARi partially reversed the reduced autophagy flux resulting from eEF2K knockdown in DIC (Fig. 7 K-N). Additionally, lysosomal acidification function was assessed using the LysoSensor Yellow/Blue probe. Our results indicated that lysosomal acidification dysfunction induced by DOX was exacerbated by eEF2K knockdown, but ARi partially reversed this lysosomal dysfunction (Fig. 7 O-P).

In conclusion, our results suggested that inhibition of GSK3β by ARi could attenuate lysosome dysfunction, alleviate autophagy blockade, and restore autophagy flux, thereby improving DIC.

## Discussion

This research reveals that myocardial eEF2K is reduced in DIC. Meanwhile, our results suggested that eEF2K ameliorated DOX-induced autophagy

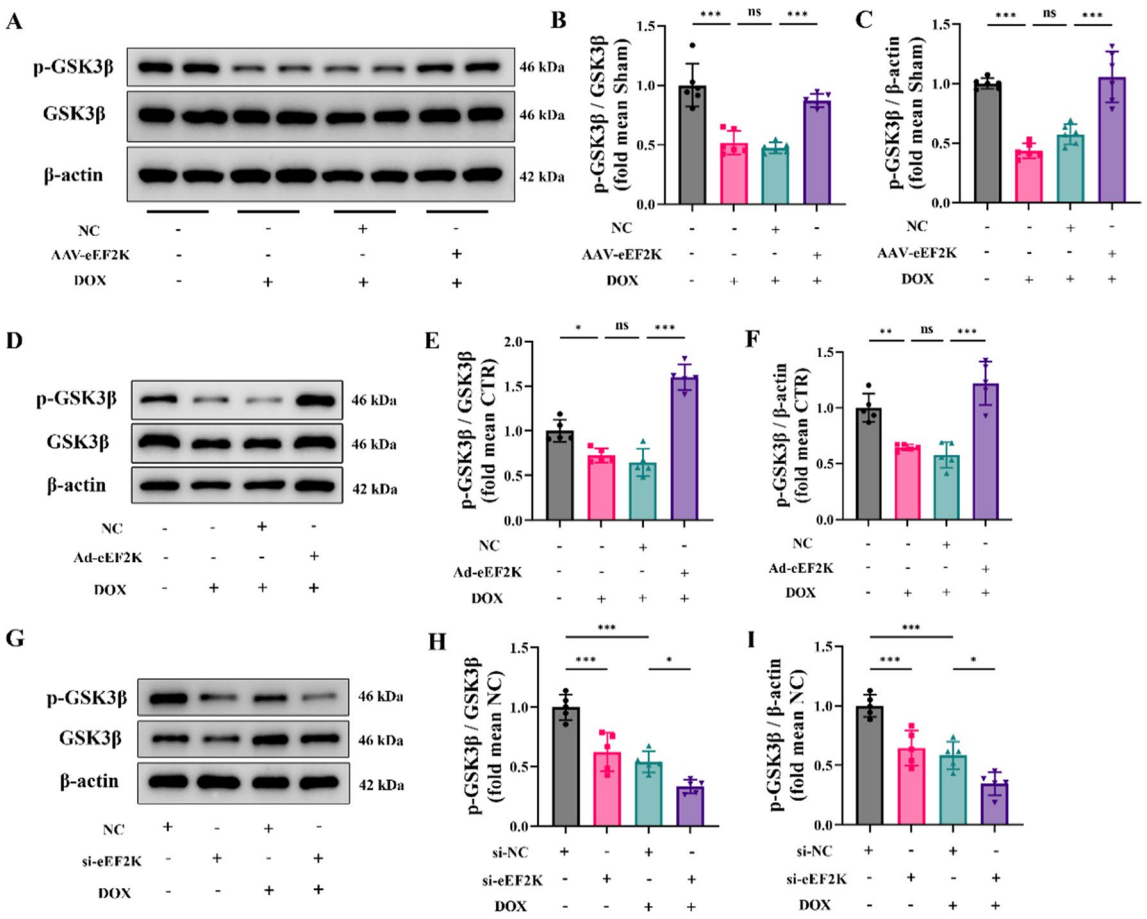


**Fig. 6** eEF2K promoted GSK3β phosphorylation in DIC. **A-C** The phosphorylation level of GSK3β at Ser9 was detected by western blot analysis in mouse hearts ($n=6$). **D-F** The phosphorylation level of GSK3β at Ser9 was detected in NRCMs following eEF2K overexpression ($n=5$). **G-I** The phosphorylation level of GSK3β at Ser9 was detected following eEF2K knockdown ($n=5$). All data are presented as mean ± standard deviation. *$p<0.05$, **$p<0.01$, ***$p<0.001$ indicate statistical differences between groups

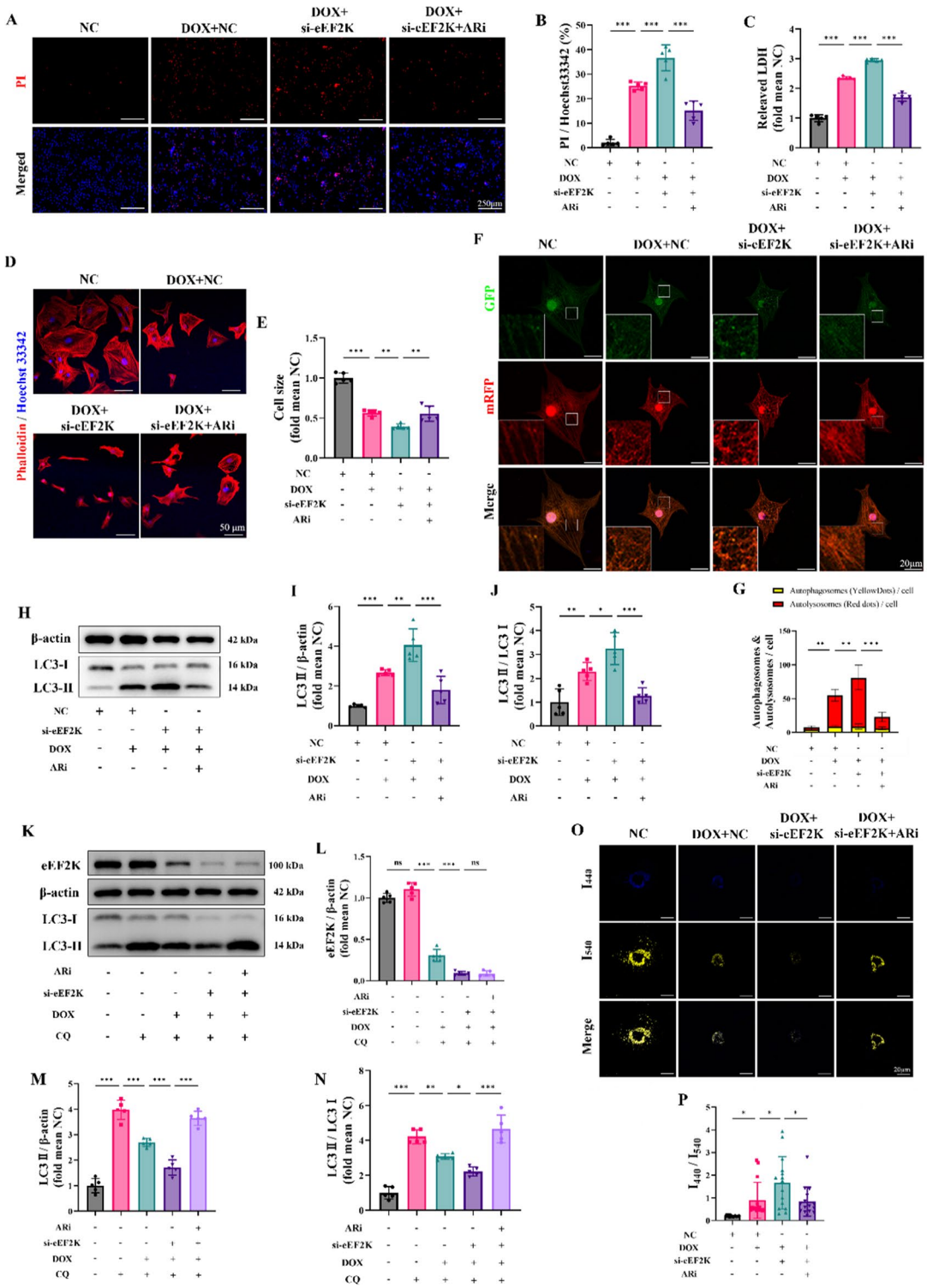
A
NC
DOX+NC
DOX+ si-eEF2K
DOX+ si-eEF2K+ARi
PI
Merged
250μm
B
PI / Hoechst33342 (%)
C
Releaved LDH (fold mean NC)
NC
DOX
si-eEF2K
ARi
D
Phalloidin / Hoechst 33342
50 μm
E
Cell size (fold mean NC)
F
GFP
mRFP
Merge
20μm
G
Autophagosomes (YellowDots) / cell
Autolysosomes (Red dots) / cell
Autophagosomes & Autolysosomes / cell
H
β-actin
LC3-I
LC3-II
42 kDa
16 kDa
14 kDa
I
LC3 II / β-actin (fold mean NC)
J
LC3 II / LC3 I (fold mean NC)
K
eEF2K
100 kDa
CQ
L
eEF2K / β-actin (fold mean NC)
M
N
O
I440
I540
P
I440 / I540

◂**Fig. 7** Inhibition of GSK3β reversed the effects of eEF2K knockdown on aggravating autophagy blockade in DIC. **A-B** Hoechst 33,342/PI staining indicated the cellular injury ($n=5$). The ratio of PI-positive cells to Hoechst 33,342-positive cells was calculated by ImageJ software to indicate the cellular injury. The scale bar represents 250 μm. **C** Myocardial cell injury was assessed by LDH detection ($n=5$). **D-E** The cardiomyocyte outline was determined by phalloidin staining. Cardiomyocyte size was quantified by ImageJ software. Hoechst 33,342 staining marks the nuclei, scale bar: 50 μm. **F-G** Representative images of NRCMs infected with mRFP-GFP-LC3 adenovirus ($n=15$). The GFP (green) is unstable in the acid organelles like lysosome while the mRFP (red) is not. Therefore, the green fluorescence of GFP quenched when the autophagosome fused with the lysosome to become autolysosome. The yellow dots merged by green dots and red dots represented autophagosomes and the red dots overlay no green dots indicated autolysosomes. The nuclei were stained with Hoechst 33,342 (blue). Scale bar: 20 μm. **H-J** LC3 were detected by western blot analysis in NRCMs ($n=5$). **K-N** LC3 were detected by western blot analysis following eEF2K knockdown, ARi and chloroquine intervention in DIC, reflecting the alteration of autophagy flux ($n=5$). **O-P** Representative fluorescence images of lysosomes using LysoSensor Yellow/Blue probes ($n=15$). The blue dots with emission peak at 440 nm representing less acidic or neutral lysosomes (impaired lysosomes) as well as the yellow dots with emission peak at 540 nm indicating acid lysosomes (functional lysosomes). The ratio of $I_{440}/I_{540}$ were measured. Scale bar: 20 μm. All data are presented as mean ± standard deviation. $^{*}p<0.05$, $^{**}p<0.01$, $^{***}p<0.001$ indicate statistical differences between groups

dysfunction by phosphorylating and inhibiting GSK3β, thereby alleviating DIC.

eEF2K was initially identified as an upstream kinase of eEF2, facilitating translation elongation by promoting the translocation of nascent peptide chains on ribosomes (Dever et al. 2018). Recognized as a therapeutic target (Kasica et al. 2022; Peng et al. 2023; Temme and Asquith 2021; Usui et al. 2013; Zhang et al. 2014), eEF2K exerts protective effects against hypoxia, glucose deprivation, and tunicamycin-induced cardiotoxicity (Kameshima et al. 2019; Pires Da Silva et al. 2020; Terai et al. 2005). Nonetheless, the possible involvement of eEF2K in DIC has not yet been investigated. In our study, we observed a decrease in the expression of eEF2K following DOX intervention in vivo, and confirmed that the effect of DOX intervention on eEF2K expression is concentration and time dependence in vitro. This finding suggests a potential involvement of eEF2K in DIC. Subsequently, adeno-associated virus was used to overexpress eEF2K, which alleviated DOX-induced cardiac dysfunction and myocardial mass loss in vivo. Simultaneously, we found that eEF2K diminished the atrophy and injury of cardiomyocytes induced by DOX in vitro.

For the biological function of eEF2K, studies have demonstrated that eEF2K regulates the cellular energy metabolism by regulating the primary energy sensor AMPK, which consequently affects the cell autophagy dynamics (Horman et al. 2002; Xie et al. 2014). Furthermore, eEF2K is acknowledged as an essential molecule in autophagy signaling when cells are under stress (Py et al. 2009). Acknowledging the effect of impaired autophagy on the pathogenesis of DIC (Bartlett et al. 2017; Dempke et al. 2023; Pan et al. 2019; Park et al. 2016; Sishi et al. 2013), we then investigated the possible role of eEF2K in controlling autophagy. In accordance with previous studies (Chen et al. 2022a; Li et al. 2016; Pan et al. 2021), we observed that DOX induced impaired autophagy flux including the lysosomal dysfunction and autolysosome accumulation. This study found that eEF2K overexpression lessened the accumulation of autophagic vacuoles caused by DOX in vivo. Meanwhile, our results indicated that eEF2K reversed DOX-induced dysfunction of autophagosome degradation by improving lysosomal function, which exerted a protective effect against DIC in vitro. These results indicated that eEF2K ameliorated DIC by promoting autophagy.

GSK3β plays a crucial role in controlling autophagy, and its reduction or inhibition can alleviate autophagy blockage and cellular damage. Madonna et al. reported that Empagliflozin significantly mitigated cardiac dysfunction in diabetic mice by inhibiting GSK3β, thereby restoring autophagy dysregulation induced by high glucose treatment (Madonna et al. 2023). Coincidentally, Su et al. found that the inhibition of Risa increased the phosphorylation of GSK3β and inhibited its activity, restoring the level of podocyte autophagy, thereby improving diabetes nephropathy (Su et al. 2022). Since DOX decreased phosphorylation of GSK3β at the Ser9 site, which increased GSK3β activity (Li et al. 2020; Su et al. 2022; Wang et al. 2021). GSK3β inhibition might ease the irregularities in autophagy associated with DIC. Interestingly, previous research indicated an association between eEF2K and GSK3β phosphorylation (Chen et al. 2022b). Our study also found that there is positive association between the eEF2K and the phosphorylation of GSK3β in DIC. Thus, it

aroused our interest in exploring whether eEF2K reversed DOX-induced autophagy dysfunction by increasing GSK3β phosphorylation and inhibiting its function. The data suggested that DOX causes a reduction in the phosphorylation level of GSK3β in mouse cardiomyocytes as well as NRCMs, while overexpression of eEF2K could restore the phosphorylation level of GSK3β. This suggested that eEF2K promoted the phosphorylation of GSK3β in DIC, leading to its functional inhibition. We then explored the impact of inhibiting GSK3β function on autophagy.

ARi, a highly selective GSK3β inhibitor, was used to investigate the potential in mitigating myocardial injury induced by eEF2K knockdown in DIC. Although eEF2K knockdown exacerbated DOX-induced autophagy blockade and lysosomal dysfunction, ARi treatment improved lysosomal function and alleviated autophagy dysfunction. Furthermore, GSK3β inhibition reversed the myocardial injury and cellular atrophy induced by eEF2K knockdown in DIC. These results indicated that eEF2K mitigated DOX-induced autophagy dysfunction by phosphorylating GSK3β and inhibiting its activity.

In summary, the cardiac expression of eEF2K was decreased by DOX, resulting in autophagy dysfunction and subsequent cardiotoxicity. eEF2K mitigates autophagy impairment by promoting the phosphorylation of GSK3β, thereby attenuating DIC. Targeted inhibition of GSK3β to mitigate autolysosome accumulation induced by DOX represents a promising novel approach warranting further investigation.

**Acknowledgements** This work was supported by the Guangdong Basic and Applied Basic Research Foundation (2024A1515012781), National Natural Science Foundation of China (82370237, 82070247), and China Postdoctoral Science Foundation under Grant (2023M741562).

**Author contributions** JG, PY, CZ and DC designed the experiments. JG, HM, VV and RG performed the animal and pathological experiments. JG, HM, VV, XZ and RG and performed the biochemical experiments. JG, DQ, WY and JY analyzed the data. JG, YW, YY and BR wrote the paper. PY, CZ and DC revised the manuscript and supervised the project. All authors have read and agreed to the published version of the manuscript.

**Funding** Guangdong Basic and Applied Basic Research Foundation (2024A1515012781), National Natural Science Foundation of China (82370237, 82070247) and China Postdoctoral Science Foundation under Grant (2023M741562).

**Data availability** Data is provided within the manuscript or supplementary information files.

**Declarations**

**Competing interests** The authors declare no competing interests.



## References

Autry AE, Adachi M, Nosyreva E, Na ES, Los MF, Cheng PF, . . ., Monteggia LM. NMDA receptor blockade at rest triggers rapid behavioural antidepressant responses. Nature. 2011;475(7354):91–95. https://doi.org/10.1038/nature10130.

Bartlett JJ, Trivedi PC, Pulinilkunnil T. Autophagic dysregulation in doxorubicin cardiomyopathy. J Mol Cell Cardiol. 2017;104:1–8. https://doi.org/10.1016/j.yjmcc.2017.01.007.

Chen D, Yu W, Zhong C, Hong Q, Huang G, Que D, . . ., Yang P. Elabela ameliorates doxorubicin-induced cardiotoxicity by promoting autophagic flux through TFEB pathway. Pharmacol Res. 2022a;178:106186. https://doi.org/10.1016/j.phrs.2022.106186.

Chen X, Wang K, Jiang S, Sun H, Che X, Zhang M, . . ., Cheng Y. eEF2K promotes PD-L1 stabilization through inactivating GSK3β in melanoma. J Immunother Cancer. 2022b;10(3). https://doi.org/10.1136/jitc-2021-004026.

Dempke WCM, Zielinski R, Winkler C, Silberman S, Reuther S, Priebe W. Anthracycline-induced cardiotoxicity - are we about to clear this hurdle? Eur J Cancer. 2023;185:94–104. https://doi.org/10.1016/j.ejca.2023.02.019.

Dever TE, Dinman JD, Green R. Translation elongation and recoding in eukaryotes. Cold Spring Harb Perspect Biol. 2018;10(8). https://doi.org/10.1101/cshperspect.a032649.

Ferreira de Souza T, Quinaglia ACST, Osorio Costa F, Shah R, Neilan TG, Velloso L, . . ., Coelho-Filho OR. Anthracycline therapy is associated with cardiomyocyte atrophy and preclinical manifestations of heart disease. JACC Cardiovasc Imaging. 2018;11(8):1045–1055. https://doi.org/10.1016/j.jcmg.2018.05.012.

Horman S, Browne G, Krause U, Patel J, Vertommen D, Bertrand L., . . ., Rider M. Activation of AMP-activated protein kinase leads to the phosphorylation of elongation factor 2 and an inhibition of protein synthesis. Curr Biol. 2002;12(16):1419–1423. https://doi.org/10.1016/s0960-9822(02)01077-1.

Hu YH, Liu J, Lu J, Wang PX, Chen JX, Guo Y, . . ., Liu PQ. sFRP1 protects H9c2 cardiac myoblasts from doxorubicin-induced apoptosis by inhibiting the Wnt/PCP-JNK pathway. Acta Pharmacol Sin. 2020;41(9):1150–1157. https://doi.org/10.1038/s41401-020-0364-z.

Hulst MB, Grocholski T, Neefjes JJC, van Wezel GP, Metsä-Ketelä M. Anthracyclines: biosynthesis, engineering and clinical applications. Nat Prod Rep. 2022;39(4):814–41. https://doi.org/10.1039/d1np00059d.

Ikeda S, Zablocki D, Sadoshima J. The role of autophagy in death of cardiomyocytes. J Mol Cell Cardiol. 2022;165:1–8. https://doi.org/10.1016/j.yjmcc.2021.12.006.

Jones DS, Podolsky SH, Greene JA. The burden of disease and the changing task of medicine. N Engl J Med. 2012;366(25):2333–8. https://doi.org/10.1056/NEJMp1113569.

Kameshima S, Kazama K, Okada M, Yamawaki H. Eukaryotic elongation factor 2 kinase mediates monocrotaline-induced pulmonary arterial hypertension via reactive oxygen species-dependent vascular remodeling. Am J Physiol Heart Circ Physiol. 2015;308(10):H1298-1305. https://doi.org/10.1152/ajpheart.00864.2014.

Kameshima S, Okada M, Yamawaki H. Eukaryotic elongation factor 2 (eEF2) kinase/eEF2 plays protective roles against glucose deprivation-induced cell death in H9c2 cardiomyoblasts. Apoptosis. 2019;24(3–4):359–68. https://doi.org/10.1007/s10495-019-01525-z.

Kasica NP, Zhou X, Jester HM, Holland CE, Ryazanov AG, Forshaw TE, . . ., Ma T. Homozygous knockout of eEF2K alleviates cognitive deficits in APP/PS1 Alzheimer's disease model mice independent of brain amyloid β pathology. Front Aging Neurosci. 2022;14:959326. https://doi.org/10.3389/fnagi.2022.959326.

Li DL, Wang ZV, Ding G, Tan W, Luo X, Criollo A, . . ., Hill JA. Doxorubicin blocks cardiomyocyte autophagic flux by inhibiting lysosome acidification. Circulation. 2016;133(17):1668–1687. https://doi.org/10.1161/circulationaha.115.017443.

Li L, Li J, Wang Q, Zhao X, Yang D, Niu L, . . ., Li Y. Shenmai injection protects against doxorubicin-induced cardiotoxicity via maintaining mitochondrial homeostasis. Front Pharmacol. 2020;11, 815. https://doi.org/10.3389/fphar.2020.00815.

Lipshultz SE, Colan SD, Gelber RD, Perez-Atayde AR, Sallan SE, Sanders SP. Late cardiac effects of doxorubicin therapy for acute lymphoblastic leukemia in childhood. N Engl J Med. 1991;324(12):808–15. https://doi.org/10.1056/nejm199103213241205.

Madonna R, Moscato S, Cufaro MC, Pieragostino D, Mattii L, Del Boccio P, . . ., De Caterina R. Empagliflozin inhibits excessive autophagy through the AMPK/GSK3β signalling pathway in diabetic cardiomyopathy. Cardiovasc Res. 2023;119(5):1175–1189. https://doi.org/10.1093/cvr/cvad009.

Orogo AM, Gustafsson ÅB. Therapeutic targeting of autophagy: potential and concerns in treating cardiovascular disease. Circ Res. 2015;116(3):489–503. https://doi.org/10.1161/circresaha.116.303791.

Pan JA, Tang Y, Yu JY, Zhang H, Zhang JF, Wang CQ, Gu J. miR-146a attenuates apoptosis and modulates autophagy by targeting TAF9b/P53 pathway in doxorubicin-induced cardiotoxicity. Cell Death Dis. 2019;10(9):668. https://doi.org/10.1038/s41419-019-1901-x.

Pan JA, Zhang H, Lin H, Gao L, Zhang HL, Zhang JF, . . ., Gu J. Irisin ameliorates doxorubicin-induced cardiac perivascular fibrosis through inhibiting endothelial-to-mesenchymal transition by regulating ROS accumulation and autophagy disorder in endothelial cells. Redox Biol. 2021;46:102120. https://doi.org/10.1016/j.redox.2021.102120.

Park JH, Choi SH, Kim H, Ji ST, Jang WB, Kim JH, . . ., Kwon SM. Doxorubicin regulates autophagy signals via accumulation of cytosolic Ca(2+) in human cardiac progenitor cells. Int J Mol Sci. 2016;17(10). https://doi.org/10.3390/ijms17101680.

Peng HY, Wang L, Das JK, Kumar A, Ballard DJ, Ren Y, . . ., Song J. Control of CD4(+) T cells to restrain inflammatory diseases via eukaryotic elongation factor 2 kinase. Signal Transduct Target Ther. 2023;8(1):415. https://doi.org/10.1038/s41392-023-01648-5.

Pires Da Silva J, Monceaux K, Guilbert A, Gressette M, Piquereau J, Novotova M, . . ., Lemaire C. SIRT1 protects the heart from ER stress-induced injury by promoting eEF2K/eEF2-dependent autophagy. Cells. 2020;9(2). https://doi.org/10.3390/cells9020426.

Piserchio A, Dalby KN, Ghose R. Revealing eEF-2 kinase: recent structural insights into function. Trends Biochem Sci. 2024;49(2):169–82. https://doi.org/10.1016/j.tibs.2023.11.004.

Py BF, Boyce M, Yuan J. A critical role of eEF-2K in mediating autophagy in response to multiple cellular stresses. Autophagy. 2009;5(3):393–6. https://doi.org/10.4161/auto.5.3.7762.

Singal PK, Iliskovic N. Doxorubicin-induced cardiomyopathy. N Engl J Med. 1998;339(13):900–5. https://doi.org/10.1056/nejm199809243391307.

Sishi BJ, Loos B, van Rooyen J, Engelbrecht AM. Autophagy upregulation promotes survival and attenuates doxorubicin-induced cardiotoxicity. Biochem Pharmacol. 2013;85(1):124–34. https://doi.org/10.1016/j.bcp.2012.10.005.

Su PP, Liu DW, Zhou SJ, Chen H, Wu XM, Liu ZS. Downregulation of Risa improves podocyte injury by enhancing autophagy in diabetic nephropathy. Mil Med Res. 2022;9(1):23. https://doi.org/10.1186/s40779-022-00385-0.

Temme L, Asquith CRM. eEF2K: an atypical kinase target for cancer. Nat Rev Drug Discov. 2021;20(8):577. https://doi.org/10.1038/d41573-021-00124-5.

Terai K, Hiramoto Y, Masaki M, Sugiyama S, Kuroda T, Hori M, . . ., Hirota H. AMP-activated protein kinase protects cardiomyocytes against hypoxic injury through attenuation of endoplasmic reticulum stress. Mol Cell Biol. 2005;25(21):9554–9575. https://doi.org/10.1128/mcb.25.21.9554-9575.2005.

Usui T, Okada M, Hara Y, Yamawaki H. Eukaryotic elongation factor 2 kinase regulates the development of hypertension through oxidative stress-dependent vascular inflammation. Am J Physiol Heart Circ Physiol. 2013;305(5):H756-768. https://doi.org/10.1152/ajpheart.00373.2013.

Wang X, Sun Q, Jiang Q, Jiang Y, Zhang Y, Cao J, . . ., Wang Y. Cryptotanshinone ameliorates doxorubicin-induced cardiotoxicity by targeting Akt-GSK-3β-mPTP pathway in vitro. Molecules. 2021;26(5). https://doi.org/10.3390/molecules26051460.

Xie CM, Liu XY, Sham KW, Lai JM, Cheng CH. Silencing of EEF2K (eukaryotic elongation factor-2 kinase) reveals AMPK-ULK1-dependent autophagy in colon cancer cells. Autophagy. 2014;10(9):1495–508. https://doi.org/10.4161/auto.29164.

Yang L, Guan J, Luo S, Yan J, Chen D, Zhang X, . . ., Yang P. Angiotensin IV ameliorates doxorubicin-induced cardiotoxicity by increasing glutathione peroxidase 4 and alleviating ferroptosis. Toxicol Appl Pharmacol. 2023;479:116713. https://doi.org/10.1016/j.taap.2023.116713.

Yeh ET, Chang HM. Oncocardiology-past, present, and future: a review. JAMA Cardiol. 2016;1(9):1066–72. https://doi.org/10.1001/jamacardio.2016.2132.

Zhang P, Riazy M, Gold M, Tsai SH, McNagny K, Proud C, Duronio V. Impairing eukaryotic elongation factor 2 kinase activity decreases atherosclerotic plaque formation. Can J Cardiol. 2014;30(12):1684–8. https://doi.org/10.1016/j.cjca.2014.09.019.

Zhang X, Hu C, Kong CY, Song P, Wu HM, Xu SC, . . ., Tang QZ. FNDC5 alleviates oxidative stress and cardiomyocyte apoptosis in doxorubicin-induced cardiotoxicity via activating AKT. Cell Death Differ. 2020;27(2):540–555. https://doi.org/10.1038/s41418-019-0372-z.

Zhong C, Que D, Yu W, Chen D, Wang Y, Zhang X, . . ., Yang P. Amine oxidase copper-containing 3 aggravates cardiac remodelling by generating hydrogen peroxide after myocardial infarction. J Pathol. 2023;260(2):190–202. https://doi.org/10.1002/path.6075.